Journal of Solid State Chemistry 181 (2008) 1882–1890

Contents lists available at ScienceDirect

Journal of Solid State Chemistry

journal homepage: www.elsevier.com/locate/jssc

New examples of ternary rare-earth metal boride carbides containing finite boron–carbon chains: The crystal and electronic structure of $RE_{15}B_6C_{20}$ (RE = Pr, Nd)

Volodymyr Babizhetskyy [a,*], Hansjürgen Mattausch [a], Arndt Simon [a], Kurt Hiebl [b], Mouna Ben Yahia [c], Régis Gautier [c], Jean-François Halet [c,*,1]

[a] Max-Planck-Institut für Festkörperforschung, Heisenbergstrasse 1, Postfach 800665, D-70569 Stuttgart, Germany
[b] Arbeitsgruppe Neue Materialien, Universität Wien, Währingerstrasse 42, A-1090 Wien, Austria
[c] Sciences Chimiques de Rennes, UMR 6226 CNRS-Ecole Nationale Supérieure de Chimie de Rennes-Université de Rennes 1, Avenue du Général Leclerc, F-35042 Rennes cedex, France

ARTICLE INFO

Article history:
Received 8 October 2007
Received in revised form
28 March 2008
Accepted 5 April 2008
Available online 12 April 2008

Dedicated to Dr. Franz Weitzer on the occasion of his 60th birthday.

Keywords:
Rare-earth metal boride carbide
Crystal structure
Electronic structure
DFT calculations
Magnetism

ABSTRACT

The ternary rare-earth metal boride carbides $RE_{15}B_6C_{20}$ (RE = Pr, Nd) were synthesized by co-melting the elements. They exist above 1270 K. Their crystal structures were determined from single-crystal X-ray diffraction data. Both crystallize in the space group $P\bar{1}$, $Z = 1$, $a = 8.3431(8)$ Å, $b = 9.2492(9)$ Å, $c = 8.3581(8)$ Å, $\alpha = 84.72(1)^\circ$, $\beta = 89.68(1)^\circ$, $\gamma = 84.23(1)^\circ$ ($R1 = 0.041$ (w$R2 = 0.10$) for 3291 reflections with $I_o > 2\sigma(I_o)$) for $Pr_{15}B_6C_{20}$, and $a = 8.284(1)$ Å, $b = 9.228(1)$ Å, $c = 8.309(1)$ Å, $\alpha = 84.74(1)^\circ$, $\beta = 89.68(1)^\circ$, $\gamma = 84.17(2)^\circ$ ($R1 = 0.033$ (w$R2 = 0.049$) for 2970 reflections with $I_o > 2\sigma(I_o)$) for $Nd_{15}B_6C_{20}$. Their structure consists of a three-dimensional framework of rare-earth metal atoms resulting from the stacking of slightly corrugated and distorted square nets, leading to cavities filled with unprecedented B_2C_4 finite chains, disordered C_3 entities and isolated carbon atoms, respectively. Structural and theoretical analyses suggest the ionic formulation $(RE^{3+})_{15}([B_2C_4]^{6-})_3([C_3]^{4-})_2(C^{4-})_2 \cdot 11\bar{e}$. Accordingly, density functional theory calculations indicate that the compounds are metallic. Both structural arguments as well as energy calculations on different boron vs. carbon distributions in the B_2C_4 chains support the presence of a CBCCBC unit. $Pr_{15}B_6C_{18}$ exhibits antiferromagnetic order at $T_N = 7.9$ K, followed by a meta-magnetic transition above a critical external field $B > 0.03$ T. On the other hand, $Nd_{15}B_6C_{18}$ is a ferromagnet below $T_C \approx 40$ K.

1. Introduction

With the impetus of Bauer and others, the chemistry of the ternary rare-earth metal boride carbides $RE_xB_yC_z$ is by now well-documented and quite well-understood [1–3]. It displays a variety of different structural arrangements with boron–carbon substructures ranging from zero-dimensional units isolated from each other in a matrix of metal atoms to one- and two-dimensional networks alternating with metal sub-lattices, which are closely related to the electron count per light atoms, boron and carbon [1–3]. Nearly a dozen of structural types have been reported so far for the most electron-rich compounds, i.e., those containing finite quasi-molecular entities [3]. These finite chains embedded in voids of the metal atom matrix can have different lengths ranging from 2 to 13 non-metal atoms up to now, and chains of different sizes as well as isolated C atom can coexist [1–3]. New structural representatives were recently discovered during our investigations of the Pr–B–C and Nd–B–C systems [4,5]. Here we report the synthesis, crystal structure, magnetic behavior and electronic structure of two of them, $Nd_{15}B_6C_{20}$ and $Pr_{15}B_6C_{20}$ which crystallize in a new structure type.

2. Experimental

2.1. Synthesis and analysis

The samples $RE_{15}B_6C_{20}$ (RE = Pr, Nd) were prepared from commercially available pure elements: rare-earth metals with a claimed purity of 99.99 at%, Alfa—Aesar, Johnson Matthey Company, sublimed bulk pieces; crystalline boron powder, purity 99.99 at%, H.C. Starck, Germany; graphite powder, purity 99.98 at%, Aldrich. Mixtures of powders in the nominal atomic ratio RE/B/C = 43/23/24 for the structural investigation were

* Corresponding authors. Fax: +49 711 689 16 42.
E-mail addresses: v.babizhetskyy@fkf.mpg.de (V. Babizhetskyy), halet@univ-rennes1.fr (J.-F. Halet).
[1] Fax: +33 2 23 23 68 40.

0022-4596/$ - see front matter © 2008 Elsevier Inc. All rights reserved.
doi:10.1016/j.jssc.2008.04.003

compacted in stainless steel dies. The pellets were arc-melted under purified argon atmosphere on a water-cooled copper hearth. The alloy buttons of ~1 g were turned over and remelted three times to improve homogeneity. Weight losses were checked to be within 1% of the original mass (1 g). Subsequent heating just above the melting point was carried out in a high-frequency furnace (TIG-10/300, Hüttinger, FRG) under purified argon atmosphere for 24 h at 1520 and 1420 K, for the Pr and Nd containing samples, respectively. Finally, the samples were wrapped in molybdenum foils, annealed in evacuated silica tubes for 1 month at 1270 K and subsequently quenched in cold water. Sample handling was carried out under argon atmosphere in a glove box or through the Schlenk technique.

Metallographic and X-ray diffraction analyses of the samples with different atomic ratios and melted in the high-frequency furnace reveal that the new compound $Pr_{15}B_6C_{20}$ is in phase equilibrium with varying amounts of $Pr_5B_2C_6$ [6] and $Pr_5B_4C_5$ [4]. Physical measurements were performed on those samples, which were contaminated by the first mentioned phase only. After annealing the samples of the phase $Pr_{15}B_6C_{20}$ at 1270 K three phases were found in equilibrium: $Pr_5B_2C_5$ [7], $Pr_5B_2C_6$ [6] and Pr [8]. The new compound $Nd_{15}B_6C_{20}$ after melting in a high-frequency furnace was found to be in phase equilibrium with $Nd_5B_2C_6$ [6] and Nd [8]. After annealing at 1270 K $Nd_{15}B_6C_{20}$ decomposed into $Nd_5B_2C_6$, Nd [8] and $Nd_5B_2C_5$ [5,9]. The temperature region of existence of $Pr_{15}B_6C_{20}$ and $Nd_{15}B_6C_{20}$ hence is higher than 1270 K. These decomposition samples are in good accordance with phase equilibria of the *RE*–B–C systems at 1270 K. The phase equilibria after annealing of $Pr_{15}B_6C_{20}$ and $Nd_{15}B_6C_{20}$ are in good accordance with sample composition and isothermal sections at 1270 K of the ternary Pr–B–C and Nd–B–C systems [4]. In particular the large C/B ratio is corroborated by the annealing experiments which result in only carbon-rich phases $RE_5B_2C_6$ and $RE_5B_2C_5$, respectively, beside elemental *RE*.

Table 1
Crystal data and structure refinement for $Pr_{15}B_6C_{20}$ and $Nd_{15}B_6C_{20}$

Empirical formula	$Pr_{15}B_6C_{20}$	$Nd_{15}B_6C_{20}$
Crystal system	Triclinic	Triclinic
Space group	$P\bar{1}$	$P\bar{1}$
Pearson symbol	aP45	aP45
Formula per unit cell, Z	1	1
Lattice parameters		
a (Å)	8.3431(8)	8.284(1)
b (Å)	9.2492(9)	9.228(1)
c (Å)	8.3581(8)	8.309(1)
α (°)	84.72(1)	84.74(1)
β (°)	89.68(1)	89.68(1)
γ (°)	84.23(1)	84.17(2)
Unit cell volume (Å^3)	639.0(2)	629.2(3)
Calculated density (g/cm^3)	6.223	6.451
Absorption coefficient (1/cm)	14.815	16.093
Crystal size (mm^3)	0.060 × 0.028 × 0.010	0.070 × 0.034 × 0.003
Radiation and wavelength (Å)	Ag $K\alpha$, 0.56086	Ag $K\alpha$, 0.56086
Diffractometer	STOE IPDS I	STOE IPDS I
Refined parameters	187	187
Refinement	F^2	F^2
$2\theta_{max}$ and $(\sin\theta/\lambda)_{max}$	47.22, 0.637	51.02, 0.697
h, k, l	$-11<h<11$	$-12<h<12$
	$-13<k<13$	$-14<k<14$
	$-11<l<11$	$-12<l<12$
Collected reflections	11,586	17,189
Independent reflections	3511 ($R_{int}=0.037$)	4349 ($R_{int}=0.069$)
Reflections with $I_o>2\sigma(I_o)$	3291($R_\sigma=0.025$)	2970($R_\sigma=0.057$)
Final R_1[a] indices (R_1[a] all data)	0.041 (0.044)	0.033 (0.066)
Weighted wR_2[b] factor(wR_2[b] all data)	[c]0.109 (0.111)	[d]0.049 (0.054)
Goodness-of-fit on F^2	1.05	1.03
Extinction coefficient	0.0097(6)	–
Largest diff. peak and hole/(e^-/Å^{-3})	3.61/−3.91	3.18/−4.00

[a] $R_1(F)=[\Sigma(|F_o|-|F_c|)]/\Sigma|F_o|$.
[b] $wR_2(F^2)=[\Sigma[w(F_o^2-F_c^2)^2/\Sigma[w(F_o^2)^2]]^{1/2}$.
[c] $[w^{-1}=\sigma^2(F_o)^2+(0.073P)^2+9.198P]$, $P=(F_o^2+2F_c^2)/3$.
[d] $[w^{-1}=\sigma^2(F_o)^2+(0.012P)^2+0.000P]$, $P=(F_o^2+2F_c^2)/3$.

2.2. X-ray diffraction and structure refinement

X-ray powder diffraction patterns were obtained on a powder diffractometer STOE STADI P with Mo$K\alpha_1$ radiation, using capillaries sealed under dried argon to avoid hydrolysis. The correct indexing and refining of X-ray powder patterns was ensured with the help of the WinCSD program package [10] and by intensity calculations taking the atomic positions from the refined structures of $Pr_{15}B_6C_{20}$ and $Nd_{15}B_6C_{20}$. The unit cell parameters refined from X-ray powder data are $a=8.355(4)$ Å, $b=9.252(3)$ Å, $c=8.376(2)$ Å, $\alpha=84.72(3)^\circ$, $\beta=89.76(4)^\circ$, $\gamma=84.23(2)^\circ$, $V=641.4(8)$ Å^3 for $Pr_{15}B_6C_{20}$ and $a=8.321(1)$ Å, $b=9.241(1)$ Å, $c=8.282(1)$ Å, $\alpha=84.33(2)^\circ$, $\beta=89.53(1)^\circ$, $\gamma=84.85(2)^\circ$, $V=631.2(3)$ Å^3 for $Nd_{15}B_6C_{20}$. The small difference between the lattice parameters determined from single crystal and powder diffraction, respectively, are quite normal.

Small and irregularly shaped single crystals were selected for X-ray investigation from crushed but not annealed samples. The crystals were first examined by Buerger precession technique in order to establish their suitability for intensity collection. Single-crystal intensity data of $RE_{15}B_6C_{20}$ (RE = Pr, Nd) were collected at room temperature on a STOE IPDS I image plate diffractometer with monochromatized Ag$K\alpha$ radiation by oscillation of the crystal around the ω-axis. All relevant crystallographic data for the data collections and evaluations are listed in Table 1. The starting atomic parameters derived via direct methods using the program SIR 97 [11] were subsequently refined with the program SHELX-97 [12] (full-matrix least-squares on F^2) with anisotropic atomic displacements within the WinGX program package [13].

The refinements converge very well for both rare-earth metal boride carbides, but they indicate the same inconsistencies. Some atomic positions are not fully occupied. The anisotropic displacement parameters of the Pr8 or Nd8 atoms show extremely large values along the c direction. We therefore refined these atoms with split positions, Pr8/Nd8 and Pr9/Nd9 with the occupation factors for Pr8 sof = 0.55(2) and for Pr9 sof = 0.45(2) in $Pr_{15}B_6C_{18}$ and Nd8 sof = 0.52(2) and Nd9 sof = 0.48(2) in $Nd_{15}B_6C_{20}$. The light atoms were located from difference Fourier maps. Refinement with boron atoms in positions C5, C6, C7 led to displacement parameters which were three times smaller compared to those of B1, B2 and B3. The result is in favor of B_2C_4 oligomers in accordance with sample composition and phase equilibria in the ternary systems *RE*–B–C (RE = Pr, Nd) at 1270 K. In both compounds the positions of C10 and C11 atoms as well display rather large isotropic displacement parameters indicating considerable defects for these sites. In the final least-square cycles these positions were refined with an occupancy factor of about 0.5 (see Tables 2 and 3) corresponding to C_3 units in two possible orientations. This disorder is associated with the split positions of surrounding *RE* atoms. The final difference Fourier analyses gave no indications for additional atomic sites.

The atomic coordinates, which correspond to their standardized form according to STRUCTURE TIDY [14] and thermal parameters are given in Tables 2–5. Selected interatomic distances are reported in Tables 6 and 7. The program DIAMOND was used for drawing crystal structures [15].

2.3. Magnetic and electric resistivity measurements

The magnetic properties were investigated in the temperature interval 1.8–330 K by use of a MPMS XL-7 SQUID magnetometer

Table 2
Atomic coordinates and isotropic displacement parameters (in Å^2) for $Pr_{15}B_6C_{20}$

Atom	Site	Occ	*x*	*y*	*z*	U_{eq}
Pr1	1*a*	1.00	0	0	0	0.0087(1)
Pr2	2*i*	1.00	0.40225(4)	0.00535(4)	0.19205(4)	0.0080(1)
Pr3	2*i*	1.00	0.26458(4)	0.36103(4)	0.26966(4)	0.0072(1)
Pr4	2*i*	1.00	0.19781(5)	0.05256(5)	0.59936(5)	0.0137(1)
Pr5	2*i*	1.00	0.06709(4)	0.36024(4)	0.86299(4)	0.0068(1)
Pr6	2*i*	1.00	0.45901(4)	0.35982(4)	0.66373(4)	0.0069(1)
Pr7	2*i*	1.00	0.12862(5)	0.65200(5)	0.53278(5)	0.0133(1)
Pr8	2*i*	0.55(2)	0.6783(3)	0.2944(9)	0.0741(2)	0.0076(6)
Pr9	2*i*	0.45(2)	0.6652(3)	0.346(1)	0.0625(3)	0.0076(8)
C1	2*i*	1.00	0.5697(9)	0.3718(8)	0.3615(9)	0.012(1)
C2	2*i*	1.00	0.2366(9)	0.6312(8)	0.2371(9)	0.013(1)
C3	2*i*	1.00	0.0378(8)	0.6233(8)	0.8365(8)	0.009(1)
C4	2*i*	1.00	0.1638(9)	0.3612(8)	0.5604(9)	0.013(1)
C5	2*i*	1.00	0.1126(8)	0.9228(8)	0.3016(9)	0.012(1)
C6	2*i*	1.00	0.5037(9)	0.0802(8)	0.4857(9)	0.012(1)
C7	2*i*	1.00	0.074(1)	0.0843(9)	0.288(1)	0.016(1)
C8	2*i*	1.00	0.314(2)	0.128(1)	0.896(2)	0.039(2)
C9	2*i*	1.00	0.621(1)	0.759(1)	0.036(2)	0.041(2)
C10	2*i*	0.5(1)	0.705(2)	0.011(2)	0.103(2)	0.018(3)
C11	2*i*	0.5(1)	0.623(3)	0.624(2)	0.025(3)	0.030(4)
B1	2*i*	1.00	0.9983(9)	0.2222(8)	0.197(1)	0.010(1)
B2	2*i*	1.00	0.558(1)	0.2151(8)	0.399(1)	0.011(1)
B3	2*i*	1.00	0.188(1)	0.7864(8)	0.237(1)	0.011(1)

Table 3
Atomic coordinates and isotropic displacement parameters (in Å^2) for $Nd_{15}B_6C_{20}$

Atom	Site	Occ	*x*	*y*	*z*	U_{eq}
Nd1	1*a*	1.00	0	0	0	0.0074(1)
Nd2	2*i*	1.00	0.40226(5)	0.00568(5)	0.19227(5)	0.00725(8)
Nd3	2*i*	1.00	0.26416(5)	0.36188(5)	0.27128(5)	0.00604(8)
Nd4	2*i*	1.00	0.19732(5)	0.05665(5)	0.59834(6)	0.01134(9)
Nd5	2*i*	1.00	0.06749(4)	0.36092(4)	0.86189(5)	0.00567(8)
Nd6	2*i*	1.00	0.45788(5)	0.36024(4)	0.66314(5)	0.00569(8)
Nd7	2*i*	1.00	0.12764(6)	0.64871(6)	0.53271(6)	0.01030(9)
Nd8	2*i*	0.52(2)	0.6785(2)	0.2936(9)	0.07416(2)	0.0054(6)
Nd9	2*i*	0.48(2)	0.6657(3)	0.347(1)	0.0622(3)	0.0070(7)
C1	2*i*	1.00	0.5719(9)	0.3706(8)	0.3628(9)	0.006(1)
C2	2*i*	1.00	0.2364(9)	0.6285(9)	0.2364(9)	0.008(1)
C3	2*i*	1.00	0.0355(9)	0.6229(8)	0.8362(8)	0.008(1)
C4	2*i*	1.00	0.1653(9)	0.3610(9)	0.5626(9)	0.006(1)
C5	2*i*	1.00	0.113(1)	0.9245(8)	0.305(1)	0.012(1)
C6	2*i*	1.00	0.502(1)	0.0809(9)	0.489(1)	0.014(2)
C7	2*i*	1.00	0.076(1)	0.085(1)	0.289(1)	0.014(1)
C8	2*i*	1.00	0.317(2)	0.127(2)	0.895(2)	0.040(5)
C9	2*i*	1.00	0.622(1)	0.759(2)	0.036(2)	0.032(5)
C10	2*i*	0.5(1)	0.705(2)	0.013(2)	0.105(2)	0.010(3)
C11	2*i*	0.5(1)	0.623(3)	0.624(2)	0.025(3)	0.018(5)
B1	2*i*	1.00	0.996(1)	0.2234(9)	0.192(1)	0.008(2)
B2	2*i*	1.00	0.561(1)	0.213(1)	0.397(1)	0.012(2)
B3	2*i*	1.00	0.194(1)	0.7857(9)	0.236(1)	0.011(2)

(Quantum Design, Inc., USA) in external fields up to 7 T. Small amounts (~10%) of the secondary phase $RE_5B_2C_6$ ($La_5B_2C_6$ type) had been observed in the samples. The crushed samples therefore had been left in air for 24 h to remove the more sensitive $RE_5B_2C_6$ phase, and about 40 mg of shiny black plate-like single crystals were selected. After that the sample handling was carried out under argon atmosphere in a glove box or through the Schlenk technique.

Measurements of the electrical resistivity were carried out for $Nd_{15}B_6C_{20}$ on the original sample containing less than approx. 10% of a secondary phase and applying a common four-probe technique in the temperature range 4.2–300 K. Electrical contacts were made with commercial silver paint (Degussa, Hanau, Germany) and 25 μm gold wire.

Table 4
Anisotropic displacement parameters in $Pr_{15}B_6C_{20}$

Atom	U_{11}	U_{22}	U_{33}	U_{23}	U_{12}	U_{13}
Pr1	0.0131(3)	0.0086(2)	0.0043(2)	−0.0006(2)	0.0008(2)	−0.0041(2)
Pr2	0.0064(2)	0.0117(2)	0.0056(2)	−0.0002(1)	−0.0002(1)	−0.0021(1)
Pr3	0.0043(2)	0.0088(2)	0.0084(2)	−0.0003(1)	−0.0002(1)	−0.0032(1)
Pr4	0.0045(2)	0.0313(3)	0.0060(2)	−0.0044(2)	−0.0017(1)	−0.0013(1)
Pr5	0.0048(2)	0.0082(2)	0.0074(2)	−0.0003(1)	0.0003(1)	−0.0024(1)
Pr6	0.0071(2)	0.0085(2)	0.0049(2)	0.0006(1)	−0.0009(1)	−0.0012(1)
Pr7	0.0063(2)	0.0296(3)	0.0037(2)	−0.0009(2)	−0.0012(2)	−0.0018(2)
Pr8	0.0045(4)	0.014(2)	0.0039(4)	−0.0011(5)	−0.0012(6)	−0.0017(3)
Pr9	0.0051(5)	0.014(2)	0.0037(5)	−0.0011(7)	−0.0013(7)	−0.0017(4)
C1	0.013(3)	0.010(3)	0.013(3)	−0.002(2)	0.001(2)	−0.002(3)
C2	0.011(3)	0.016(3)	0.012(3)	−0.001(3)	0.001(3)	−0.002(3)
C3	0.008(3)	0.013(3)	0.005(3)	−0.004(2)	0.002(2)	−0.003(2)
C4	0.012(3)	0.016(3)	0.012(3)	−0.004(3)	0.003(3)	−0.004(3)
C5	0.006(3)	0.012(3)	0.019(3)	−0.003(2)	0.004(2)	0.002(3)
C6	0.009(3)	0.014(3)	0.013(3)	0.003(2)	−0.001(2)	0.002(3)
C7	0.018(3)	0.015(3)	0.014(3)	0.000(3)	−0.003(3)	−0.003(3)
B1	0.009(3)	0.009(3)	0.020(4)	−0.008(3)	−0.003(2)	0.002(3)
B2	0.013(3)	0.008(3)	0.013(3)	−0.003(2)	−0.002(2)	−0.004(3)
B3	0.011(3)	0.011(3)	0.014(3)	−0.002(3)	−0.003(2)	−0.006(3)

Table 5
Anisotropic displacement parameters in $Nd_{15}B_6C_{20}$

Atom	U_{11}	U_{22}	U_{33}	U_{23}	U_{12}	U_{13}
Nd1	0.0116(3)	0.0066(2)	0.0040(2)	−0.0007(2)	−0.0001(2)	−0.0025(2)
Nd2	0.0068(2)	0.0099(2)	0.0046(2)	−0.0003(1)	0.0001(1)	−0.0012(1)
Nd3	0.0045(2)	0.0065(2)	0.0071(2)	−0.0008(1)	−0.0003(1)	−0.0017(1)
Nd4	0.0049(2)	0.0246(2)	0.0051(2)	−0.0037(1)	−0.0020(1)	0.0001(1)
Nd5	0.0049(2)	0.0058(2)	0.0061(2)	−0.0006(1)	−0.0001(1)	−0.0010(1)
Nd6	0.0069(2)	0.0061(2)	0.0042(2)	−0.0000(1)	−0.0014(1)	0.0000(1)
Nd7	0.0061(2)	0.0213(2)	0.0036(2)	−0.0012(1)	−0.0019(1)	−0.0005(1)
Nd8	0.0042(4)	0.010(2)	0.0029(4)	−0.0014(5)	−0.0022(6)	−0.0004(3)
Nd9	0.0059(4)	0.011(2)	0.0040(4)	−0.0015(6)	−0.0023(6)	0.0004(3)
C1	0.007(3)	0.006(3)	0.006(3)	−0.003(2)	−0.001(2)	−0.002(3)
C2	0.010(3)	0.004(3)	0.010(3)	−0.001(2)	−0.002(2)	−0.004(3)
C3	0.013(3)	0.009(3)	0.003(3)	0.001(2)	−0.002(3)	0.001(3)
C4	0.010(2)	0.015(3)	0.004(3)	0.001(2)	0.001(2)	−0.001(2)
C5	0.012(3)	0.013(4)	0.009(3)	0.001(3)	−0.004(3)	−0.004(3)
C6	0.011(4)	0.015(4)	0.014(4)	0.001(3)	0.000(3)	0.003(3)
C7	0.013(4)	0.021(4)	0.007(4)	−0.001(3)	−0.004(3)	−0.006(3)
B1	0.004(3)	0.009(4)	0.011(4)	−0.006(3)	0.003(3)	0.002(3)
B2	0.007(3)	0.019(4)	0.011(4)	−0.005(3)	0.002(3)	−0.002(3)
B3	0.022(4)	0.005(3)	0.007(4)	0.002(3)	−0.007(3)	0.003(3)

2.4. Theoretical calculations

Self-consistent *ab initio* spin polarized band structure calculations were carried out on $Pr_{15}B_6C_{20}$ with the scalar relativistic tight-binding linear muffin-tin orbital method in the atomic spheres approximation including the combined correction (LMTO) [16]. Exchange and correlation were treated in the local density approximation using the von Barth–Hedin local exchange correlation potential [17]. Within the LMTO formalism, interatomic space is filled with interstitial spheres. The optimal positions and radii of these additional "empty spheres" (ES) were determined by the procedure described in Ref. [18]. A number of 59 non-symmetry related ES with $0.57 \leqslant r_{ES} \leqslant 1.18$ Å were introduced for the calculations. The full LMTO basis set consisted of 6*s*, 6*p*, 5*d* and 4*f* functions for Pr spheres, 2*s*, 2*p* and 3*d* functions for B and C spheres, and *s*, *p* and *d* functions for ES. The eigenvalue problem was solved using the following minimal basis set obtained from the Löwdin downfolding technique: Pr (6*s*, 5*d*, 4*f*), B (2*s*, 2*p*), C (2*s*, 2*p*), and ES (1*s*). The *k* space integration was performed using the tetrahedron method [19]. Charge self-consistency and the average

Table 6
Selected interatomic distances (Å) in $Pr_{15}B_6C_{20}$

Atoms	Distance	Atoms	Distance	Atoms	Distance
Pr1–2C10	2.59(2)	Pr4–C10	2.61(2)	Pr7–C4	2.584(8)
2C7	2.692(8)	C5	2.710(7)	C2	2.643(8)
2C5	2.703(8)	C6	2.746(8)	C3	2.644(7)
2B1	2.751(8)	C6	2.784(8)	C1	2.653(8)
2B3	2.998(8)	2C7	2.820(8)	C4	2.663(7)
2Pr5	3.5202(4)	C4	2.831(7)	B3	2.726(8)
2Pr8	3.718(6)	C8	2.84(1)	B1	2.787(8)
2Pr2	3.7349(4)	Pr7	3.7532(6)	Pr8	3.762(2)
2Pr4	3.7381(4)	Pr5	3.8272(6)	Pr7	3.7845(6)
		Pr6	3.8282(6)	Pr9	3.805(3)
Pr2–2C10	2.64(2)	Pr7	3.8963(7)		
2C8	2.69(1)	Pr4	3.9501(6)	Pr8–C10	2.60(2)
C5	2.733(7)			C11	2.66(3)
C9	2.75(1)	Pr5–C3	2.409(7)	C3	2.690(8)
C6	2.769(8)	C4	2.650(8)	C1	2.695(8)
C6	2.830(8)	C2	2.663(8)	C2	2.737(8)
B3	2.831(8)	C3	2.667(7)	C9	2.77(1)
C7	2.893(8)	C11	2.79(3)	B1	2.861(8)
Pr3	3.4910(5)	B3	2.808(8)	B2	2.948(9)
Pr6	3.5611(5)	C8	2.81(1)	B3	2.956(9)
Pr2	3.5976(5)	C9	2.82(1)	C11	3.02(2)
Pr4	3.7408(6)	Pr6	3.6611(5)		
Pr8	3.762(6)	Pr5	3.6961(5)	Pr9–C11	2.49(3)
Pr8	3.823(6)	Pr7	3.7132(5)	C11	2.54(2)
Pr4	3.8404(5)	Pr9	3.744(3)	C2	2.627(8)
		Pr7	3.7490(6)	C1	2.643(8)
Pr3–C2	2.474(7)	Pr8	3.760(3)	C3	2.671(7)
C4	2.567(8)	Pr9	3.780(7)	C9	2.83(1)
C11	2.62(3)			C10	3.07(2)
C3	2.665(7)	Pr6–C1	2.459(7)	Pr9	3.83(1)
C1	2.678(8)	C4	2.612(8)		
B1	2.770(8)	C1	2.682(8)	C1–B2	1.47(1)
B2	2.845(8)	C2	2.688(8)		
Pr7	3.6722(6)	C11	2.71(3)	C2–B3	1.45(1)
Pr6	3.6782(5)	C9	2.75(1)		
Pr5	3.6887(5)	B2	2.768(8)	C3–B1	1.43(1)
Pr6	3.7108(5)	Pr6	3.7029(5)		
Pr7	3.7166(6)	Pr9	3.746(3)	C5–C7	1.49(1)
Pr9	3.752(3)	Pr7	3.7537(6)	B3	1.50(1)
Pr9	3.781(7)	Pr9	3.776(7)		
Pr5	3.7864(5)	Pr7	3.8001(6)	C6–C6	1.49(1)
Pr8	3.830(3)	Pr8	3.866(2)	B2	1.49(1)
Pr4	3.8600(6)				
C7–B1	1.50(1)	C8–C9	1.38(2)		
C8–C10	1.32(2)	C9–C11	1.27(2)		

Table 7
Selected interatomic distances (Å) in $Nd_{15}B_6C_{20}$

Atoms	Distance	Atoms	Distance	Atoms	Distance
Nd1–2C10	2.58(2)	Nd3–Nd5	3.781(1)	Nd6–Nd7	3.711(1)
2C7	2.701(9)	Nd4	3.811(1)	Nd9	3.731(3)
2C5	2.709(9)	Nd8	3.814(2)	Nd9	3.753(7)
2B1	2.718(9)			Nd7	3.788(1)
2B3	2.990(9)	Nd4–C10	2.60(2)	Nd8	3.850(2)
2Nd5	3.520(1)	C5	2.683(9)		
2Nd8	3.695(6)	C6	2.700(9)	Nd7–C4	2.570(8)
2Nd2	3.711(1)	C7	2.736(9)	C3	2.623(8)
2Nd4	3.725(1)	C4	2.780(8)	C1	2.624(8)
		C6	2.802(9)	C2	2.631(8)
Nd2–C10	2.62(2)	C8	2.82(2)	C4	2.634(8)
C8	2.64(2)	C7	2.838(9)	B3	2.733(9)
C10	2.66(2)	Nd7	3.719(1)	B1	2.810(9)
C8	2.68(2)	Nd6	3.784(1)	Nd7	3.711(1)
C5	2.717(9)	Nd5	3.785(1)	Nd8	3.754(2)
C9	2.74(1)	Nd4	3.940(1)	Nd9	3.790(3)
C6	2.776(9)	Nd7	3.952(1)		
C6	2.790(9)			Nd8–C10	2.57(2)
B3	2.816(9)	Nd5–C3	2.399(7)	C1	2.683(8)
C7	2.860(9)	C4	2.613(8)	C3	2.692(9)
Nd3	3.488(1)	C2	2.643(8)	C11	2.70(3)
Nd6	3.559(1)	C3	2.661(8)	C2	2.723(9)
Nd2	3.579(1)	C11	2.70(3)	C9	2.77(1)
Nd4	3.722(1)	C9	2.80(1)	C1	2.811(9)
Nd8	3.742(5)	B3	2.80(1)	C2	2.91(1)
Nd8	3.807(6)	C8	2.83(1)	C3	2.92(1)
Nd4	3.815(1)	Nd6	3.622(1)	C11	3.03(2)
		Nd7	3.676(1)		
Nd3–C2	2.440(8)	Nd5	3.684(1)	Nd9–C11	2.54(3)
C4	2.549(8)	Nd7	3.702(1)	C11	2.54(2)
C11	2.62(3)	Nd9	3.722(3)	C2	2.605(9)
C3	2.629(8)	Nd8	3.744(2)	C1	2.633(8)
C1	2.676(8)	Nd9	3.751(7)	C3	2.667(9)
B1	2.779(8)			C9	2.83(2)
B2	2.85(1)	Nd6–C1	2.461(7)	C10	3.05(2)
Nd7	3.629(1)	C4	2.566(8)	Nd9	3.80(1)
Nd6	3.636(1)	C1	2.660(8)		
Nd5	3.661(1)	C11	2.68(3)	C1–B2	1.47(1)
Nd7	3.664(1)	C2	2.683(8)		
Nd6	3.694(1)	C9	2.74(1)	C2–B3	1.46(1)
Nd9	3.740(3)	B2	2.78(1)		
Nd9	3.762(7)	Nd6	3.682(1)	C3–B1	1.41(1)
C5–C7	1.47(1)	C6–B2	1.50(1)	C8–C10	1.33(2)
B3	1.53(1)			C9	1.36(2)
		C7–B1	1.54(1)		
C6–C6	1.49(1)			C9–C11	1.25(2)

properties were obtained from 63 irreducible k points. The density of states (DOS) curves were shifted to position the Fermi level at 0 eV. Spin polarization was taken into account in order to allow convergence with the f elements.

Alternatively extended Hückel tight-binding [20] calculations were carried out using the program YAeHMOP [21]. The exponents (ζ) and the valence shell ionization potentials (H_{ii} in eV) were respectively: 1.3, −15.2 for B 2s; 1.3, −8.5 for B 2p; 1.625, −21.4 for C 2s; 1.625, −11.4 for C 2p and 1.4, −4.86 for Pr 6s and 6p. The H_{ii} value for Pr 5d was at −6.06. A linear combination of two Slater-type orbitals with exponents $\zeta_1 = 2.747$ and $\zeta_2 = 1.267$ with the weighting coefficients $c_1 = 0.718$ and $c_2 = 0.445$ were used to represent the Pr 5d atomic orbitals.

3. Results and discussion

3.1. Structural characterization

Although $RE_{15}B_6C_{20}$ (RE = Pr, Nd) crystallizes in a new type of structure, it is closely related to the crystal structures of other ternary praseodymium and neodymium boride carbides containing isolated boron–carbon chains of different lengths such as in $RE_5B_2C_6$ [6] ($La_5B_2C_6$ structure-type [22]), $RE_5B_2C_5$ [7,9] ($Gd_5B_2C_5$ structure-type [9]), RE_2BC (Nd_2BC structure type [23]) or $RE_5B_4C_5$ [4,5] ($Ce_5B_4C_5$ structure-type [24]). The rare-earth metal sublattice consists of a three-dimensional framework resulting from the stacking of slightly corrugated and distorted square nets along the [001] direction and rotated to each other by about 45° (Fig. 1, left). Pr–Pr and Nd–Nd distances between the nets range from 3.4910(5) Å (Pr2–Pr3) to 3.8963(7) Å (Pr4–Pr7) and from 3.488(1) Å (Nd2–Nd3) to 3.719(1) Å (Nd4–Nd7), respectively. Within the nets, Pr–Pr and Nd–Nd separations are somewhat longer, between 3.5976(5) Å (Pr2–Pr2) and 3.9501(6) Å (Pr4–Pr4), respectively (see Table 6), and between 3.579(1) Å (Nd2–Nd2) and 3.952(1) Å (Nd4–Nd7), respectively (see Table 7). Such a stacking along the c direction leads to the formation of three different types of cavities: octahedral, distorted bicapped square-antiprismatic and distorted bicapped double antiprismatic cavities encapsulating isolated carbon atoms, disordered C_3 chains formed by C8, C9, C10 and C11 atoms and unprecedented finite B_2C_4 oligomers, respectively (see Fig. 1).

The isolated C4 atoms in $RE_{15}B_6C_{20}$ occupy the centers of slightly distorted metal atom octahedra (Fig. 1c). RE–C separations in the octahedral voids range from 2.567(8) Å (Pr3–C4) to

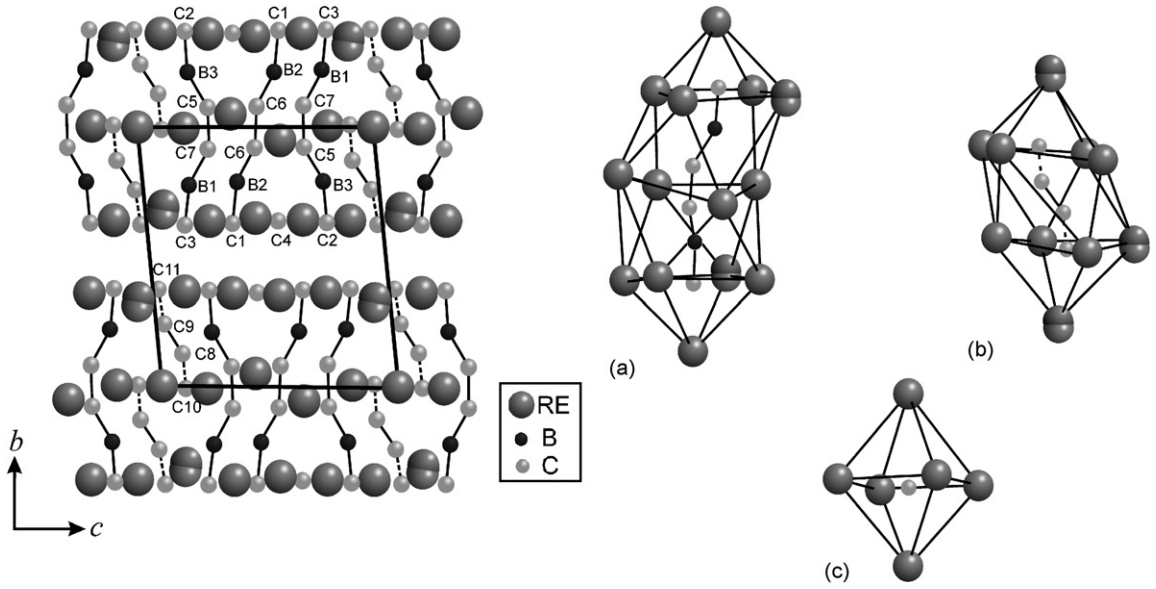

Fig. 1. Crystal structure of $RE_{15}B_6C_{20}$ along [100] (left) and rare-earth metal environments of the B_2C_4 chains (a), disordered C_3 units (b) and isolated carbon atoms (c).

2.831(7) Å (Pr4–C4) and from 2.549(8) Å (Nd3–C4) to 2.780(8) Å (Nd4–C4) for *RE* = Pr and Nd, respectively (Tables 6 and 7).

The C atoms C8–C11 of the disordered C_3 units are surrounded by 10 *RE* atoms which form a distorted bicapped square antiprism (Fig. 1b). Such a metal atom cage has already been encountered in other rare-earth metal boride carbides. It generally contains tri-atomic chains such as BC_2 in $RE_5B_2C_5$ [6,7,9], or four-atomic chains such as BC_3 in $RE_5B_2C_6$ [22] and B_2C_2 in Nd_2BC [23], rather than C_2 units which generally occupy distorted octahedral voids [1–3]. The C_3 entity is formed by C8–C11 with positions C10 and C11 that are partially occupied in both compounds. These partial occupations are accompanied by pronounced disorder of the Pr8/Pr9 (Nd8/Nd9) atoms. These results suggest (a) two disordered C_3 groups C8–C9–C10 and C8–C9–C11 in the ratio 1:1 or (b) three disordered C_2 groups C10–C8, C8–C9, C9–C11 (1:1:1). Unambiguous location of $2 \times$ C3-groups or $2 \times$ C2-groups is not obvious from the X-ray measurements. However, the occupation of such large voids by only small C_2 units is highly improbable. The observation of large displacement parameters for the central atoms C8 and C9 is in line with the proposed disorder of C_3 units. Disordered tri-atomic entities in the same kind of voids are also known from $La_5B_2C_6$ [22]. Hence, we suggest that the title compounds contain C_3 chains analogous to those found in Sc_3C_4, Ho_4C_7 and Y_4C_7 [25,26]. No longer carbon chains have been reported in solid state compounds so far. The C–C distances range from 1.27(2) Å (C9–C11) to 1.38(2) Å (C8–C9) in $Pr_{15}B_6C_{20}$, and from 1.25(2) Å (C9–C11) to 1.36(2) Å (C8–C9) in $Nd_{15}B_6C_{20}$. The short atom distances between light atoms exclude alternative units, e.g. BC_2. Bond angles in the chain C11–C9–C8–C10 are $\varphi_{C11-C9-C8} = 148.9(1)^\circ$ and $\varphi_{C9-C8-C10} = 150.8(1)^\circ$. Comparable C–C distances are observed for Pr and Nd binary carbides [27,28]. The deviation from linearity in the chain C11–C9–C8–C10 is somewhat more pronounced than in the B_2C_4 units where bond angles range from 150.1(7)° ($\varphi_{C5-C7-B1}$) to 157.6(3)° ($\varphi_{C1-B2-C6}$) or in the BC_3 chain in $Pr_5B_2C_6$ [6] where the average bond angles $\varphi_{C1-C2/B2-C2/B2}$ are 155.8°.

Three B_2C_4 units are located in the unit cell; one symmetrical (C1–B2–C6–C6–B2–C1) and two asymmetrical (C2–B3–C5–C7–B1–C3 and C3–B1–C7–C5–B3–C2). B–C distances range from 1.43(1) to 1.50(1) Å and C–C distances are 1.49(1) Å in $Pr_{15}B_6C_{20}$ (Table 6). Nearly similar bond lengths are measured for $Nd_{15}B_6C_{20}$ with B–C distances ranging from 1.41(1) to 1.54(1) Å and C–C distances being between 1.47(1) and 1.49(1) (Table 7). Those distances are typically found for other related rare-earth metal boride carbides containing finite boron–carbon chains [1–3]. Distances normally lie in the following ranges: B–C = 1.45–1.52 Å, C–C = 1.25–1.48 Å and B–B = 1.56–1.66 Å. To mention actual examples, the B–B distances found in six-membered chains B_3C_3 have 1.57 Å [24] or range from 1.59 Å in the longer chains B_5C_8 to 1.62 Å in B_4C_4 [29].

Unambiguous location of B and C atoms in this kind of compound is not obvious only from X-ray measurements, but often decided on the basis of the chemical environment, the electronegativity of boron vs. carbon and also theoretical considerations [1–3,29]. With respect to this point, one structural aspect needs to be addressed: the boron vs. carbon distribution in the B_2C_4 chains (C–B–C–C–B–C, as experimentally proposed, or C–C–B–B–C–C). The rather even distribution of distances is in favor of a central C–C unit. One could try to substantiate this assignment further by analyzing the C/B–*RE* bond length. However, such an analysis is hampered by the split positions in the *RE* atom positions around the B_2C_4 unit and do not lead to an unambiguous result. Crystallographically measured distances indicate double bond character for all the B–C and/or C–C bonds. This implies a cumulene-like molecule $[B_2C_4]^{6-}$, regardless of the atomic distribution and a $[C_3]^{4-}$ unit. This leads to the charge distribution $(RE^{3+})_{15}([B_2C_4]^{6-})_3[C_3]^{4-}_2(C^{4-})_2 \cdot 11\bar{e}$ in an ionic limit.

3.2. Electronic structure

Periodic density functional calculations of the LMTO type (see computational details) were carried out in order to address first the atomic "coloring" in the B_2C_4 chains, as well as to get some insight into the electronic structure of the title compounds. Calculations for $Pr_{15}B_6C_{18}$ and $Nd_{15}B_6C_{18}$ led to similar results. Consequently, only the results obtained for the former are commented here. Calculations were first performed on the ordered experimental structure with C–B–C–C–B–C distribution and C_3 units formed by C8, C9 and C10. A comparison of the total electronic energy indicates that $Pr_{15}B_6C_{20}$ is more stable with the

experimentally proposed C–B–C–C–B–C distribution than with the hypothetical C–C–B–B–C–C distribution by 0.12 eV per unit cell. This indicates that B–B bonds are unlike in $Pr_{15}B_6C_{20}$. The energy difference computed for the two arrangements is sufficiently substantial to propose that the compounds $RE_{15}B_6C_{20}$ contain C–B–C–C–B–C chains.

The total DOS of $Pr_{15}B_6C_{20}$ on the basis of the X-ray structure and the above interpretation is shown in Fig. 2, together with projections on the orbitals of Pr atoms, B_2C_4 and C_3 units as well as the isolated C atoms. As expected from the ionic limit (see above), with not fully oxidized rare-earth metals, the title compounds should be metallic in character (*vide infra*) with the Fermi level E_F lying in a pronounced peak of DOS from all the constituting elements. The Pr projected DOS shows the presence of metal atom contribution below the Fermi level E_F which reflects some substantial metal–ligand (B_2C_4, C_3 and C) covalent interaction. This is supported by the fragment net charges computed at the EH-TB level, $(Pr^{2.08+})_{15}([B_2C_4]^{6.11-})_3([C_3]^{3.64-})_2(C^{2.81-})_2$.

3.3. Magnetic properties

The results of the magnetic measurements carried out on $RE_{15}B_6C_{20}$ (RE = Pr, Nd) are summarized in Figs. 3–6. The reciprocal susceptibilities vs. temperature are shown in Figs. 3–4. The measured data follow an almost linear Curie–Weiss law above 50 K and were least squares fitted using the formula

$$\chi = \frac{C}{T-\theta_p} + \chi_0 \quad (1)$$

C being the Curie constant and χ_0 ($\sim 10^{-9}\,m^3/mol$) denoting temperature-independent contributions such as core diamagnetism, Landau diamagnetism and Pauli-type paramagnetism. The derived values for the effective moments, $\mu_{eff} = 3.60\,\mu_B$/Pr and $\mu_{eff} = 3.64\,\mu_B$/Nd, agree well with the theoretical moments of the respective RE^{3+} ions. The paramagnetic Curie temperatures, θ_p, were found to be 13.8 and 14.2 K, for the Pr and Nd compounds, respectively, indicating ferromagnetic type of coupling.

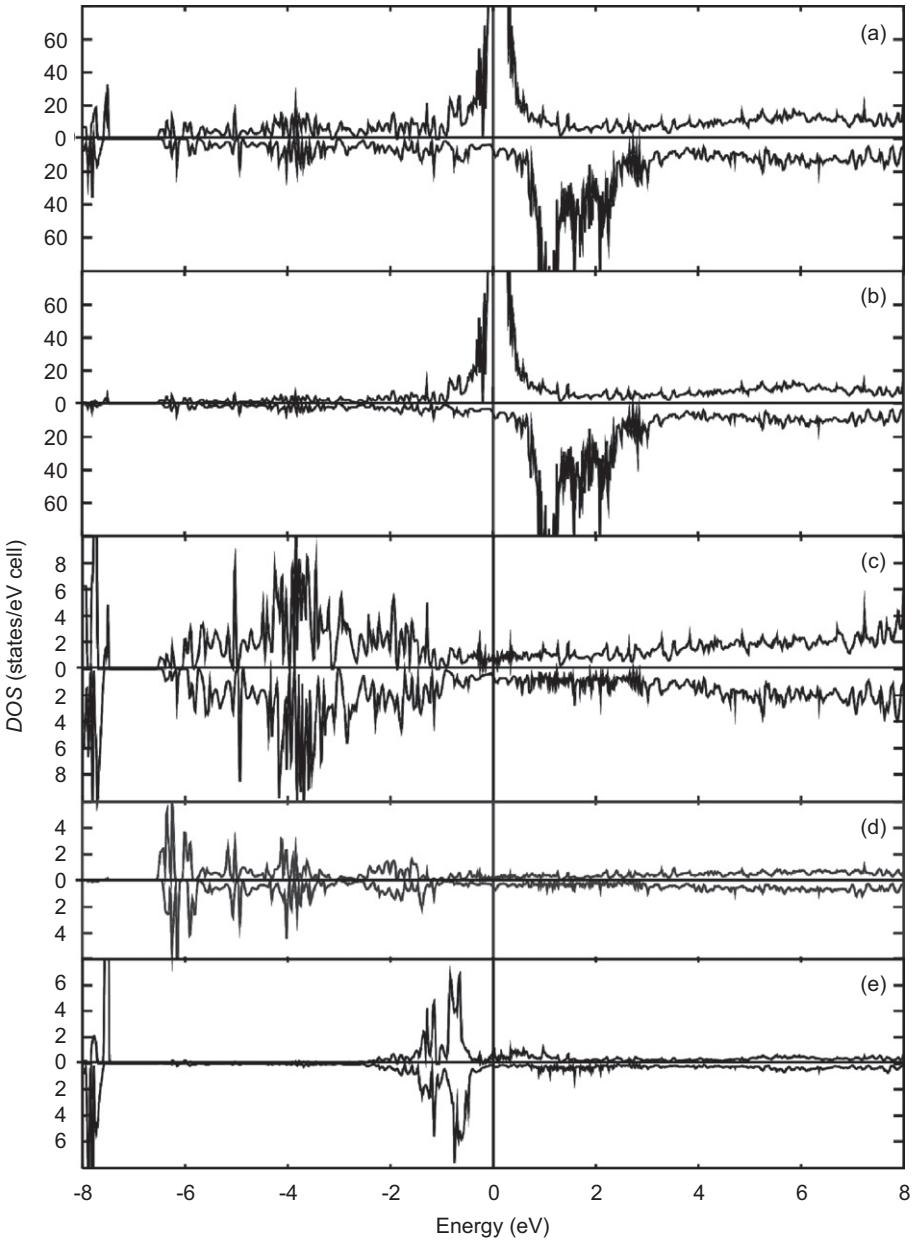

Fig. 2. Spin polarized DOS of $Pr_{15}B_6C_{20}$: (a) total, (b) Pr contribution, (c) B_2C_4 contribution, (d) C_3 contribution and (e) C contribution.

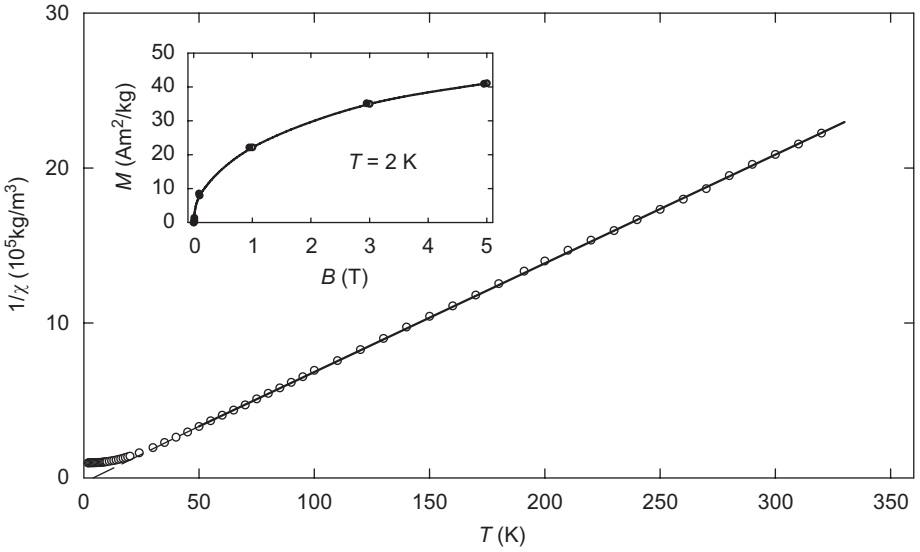

Fig. 3. Reciprocal susceptibility vs. temperature for $Pr_{15}B_6C_{20}$ at $B = 7$ T. Full and dashed line: least squares fit after Eq. (1). *Inset*: isothermal magnetization vs. magnetic field at $T = 2$ K.

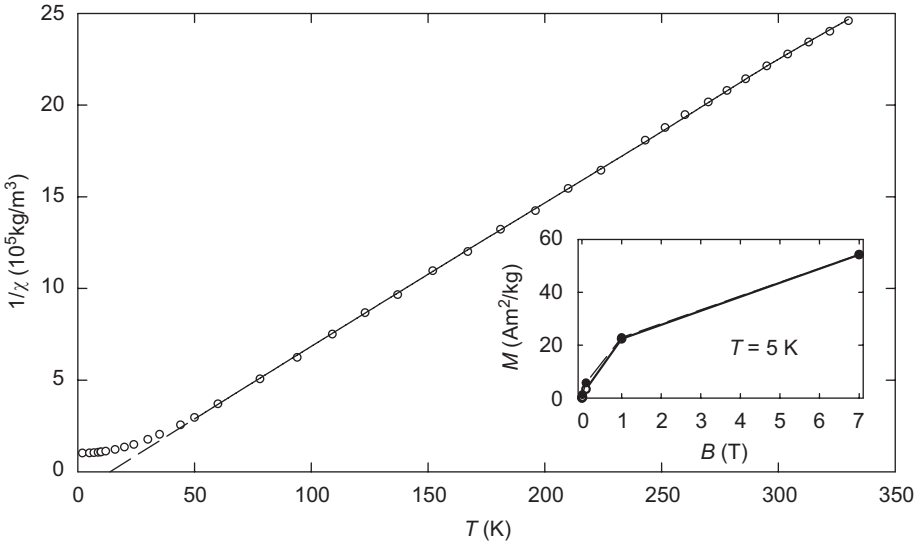

Fig. 4. Reciprocal susceptibility vs. temperature for $Nd_{15}B_6C_{20}$ at $B = 7$ T. Full and dashed line: least squares fit after Eq. (1). *Inset*: Isothermal magnetization vs. magnetic field at $T = 5$ K.

Upon lowering the temperature both samples undergo magnetic transitions. The $\chi(T)$ plot (see Fig. 5) of $Pr_{15}B_6C_{18}$ reveals a pronounced maximum at a Néel temperature $T_N = 8$ K for measurements of zero field cooled (zfc) as well as of field cooled (fc) samples, i.e., in increasing or decreasing temperatures, in an external field $B = 0.01$ T. We attribute this behavior to an anti-parallel spin alignment of the praseodymium sub-lattice. Above a critical field $B > 0.03$ T a meta-magnetic transition towards parallel spin alignment is observed. The susceptibilities in external fields $B = 0.1$ and 1 T show the characteristic saturation effects for ferromagnets below $T = 5$ K (Fig. 5). From isothermal magnetization curves vs. applied magnetic fields at $T = 2$ K, a saturation moment $\mu_S = 1.52\,\mu_B$ at $B = 7$ T is derived as can be seen in the inset of Fig. 3. On the other hand, the results of the magnetic measurements of the compound $Nd_{15}B_6C_{20}$ are somewhat different when compared with those of $Pr_{15}B_6C_{20}$ ones. The $\chi(T)$ plots in low external field, $B = 0.1$ T reveal a pronounced difference depending on the sample treatment prior to measurement as shown in Fig. 6. Such a magnetization process in the ordered state is commonly attributed to the presence of narrow domain walls [30]. The net magnetization of zfc samples increases when rising the temperature due to thermal activation of the domain wall movement, reaches a maximum and falls off to small values at the ordering temperature $T_C = 40$ K, whereas a high net magnetization is frozen when the sample is fc in decreasing temperature. The origin of the presence of narrow domain walls is a high magneto-crystalline energy. In higher fields ($B > B_{crit} > 1$ T) the difference of the $\chi(T)$ plots in increasing and decreasing fields are negligible. From isothermal magnetization curves vs. applied magnetic fields at $T = 5$ K a saturation moment $\mu_S = 1.60\,\mu_B$ at $B = 7$ T is observed (see the inset of Fig. 4). The reduced values of the saturation moments $\mu_S = 1/2\,gJ$ are possibly due to a non-collinear spin alignment of the ordered moments in these compounds crystallizing in a space group of low symmetry. Also, the influence of crystalline field effects (splitting of the $^4I_{9/2}$ multiplet in the "quasi-tetragonal symmetry") must not be

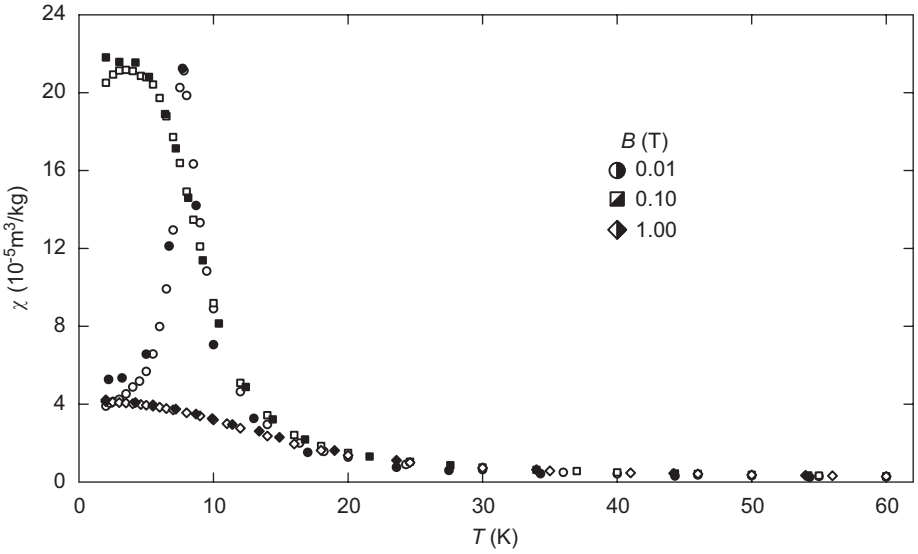

Fig. 5. Susceptibility vs. temperature for $Pr_{15}B_6C_{20}$ at various magnetic fields.

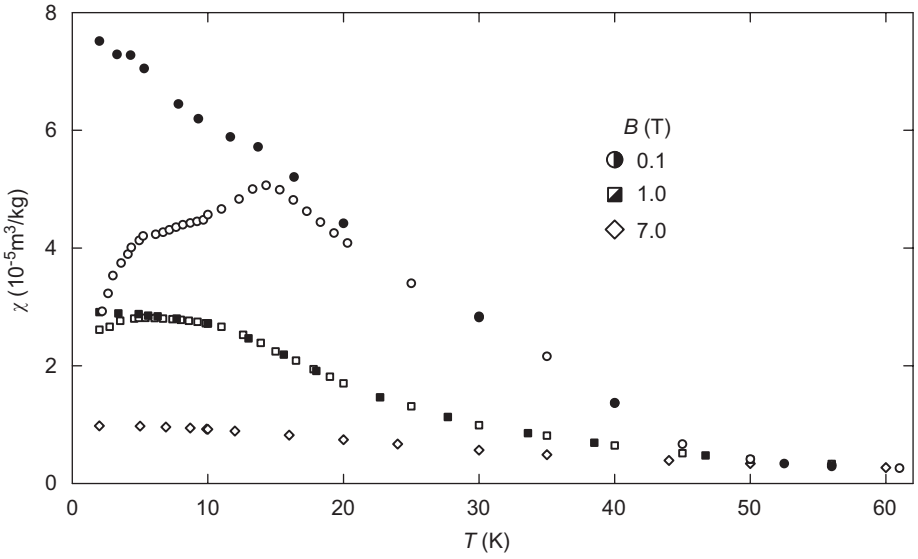

Fig. 6. Susceptibility vs. temperature for $Nd_{15}B_6C_{20}$ at various magnetic fields.

excluded. A rough de Gennes scaling of the Curie temperatures indicates the indirect exchange interaction (*RKKY*-interaction) as the driving force for the magnetic coupling.

3.4. Electrical resistivity

The normalized electrical resistivity of $Nd_{15}B_6C_{20}$ is plotted as a function of temperature in Fig. 7. The overall shape of the $\rho(T)$ curve is reminiscent of the behavior of a magnetic metal. Starting at room temperature the resistivity decreases upon lowering the temperature due to the temperature dependent electron–phonon interaction. Below the ferromagnetic ordering temperature, of approx. 40 K in good agreement with the magnetic data, a characteristic change of the slope of the $\rho(T)$ curve owing to the additional contribution of the spin wave scattering of the conduction electrons in the ordered state is encountered. In particular, a T^2 dependence for the spin wave contribution to the total resistivity in ferromagnetic materials was derived by Kasuya [31]. We have fitted our data at low temperatures according to the general formula $\rho(T) = \rho_0 + AT^2 = 0.8 + 3.06 \times 10^{-5}\ T^2$, and the results are shown in Fig. 7 as the dashed line.

4. Conclusion

The compounds $RE_{15}B_6C_{20}$ (RE = Pr, Nd) can be prepared at high temperatures by arc-melting and subsequent remelting in a high-frequency furnace from the elements. The temperature region of existence of such phases is higher than 1270 K. Their structure consists of a three-dimensional framework of rare-earth metal atoms resulting from the stacking of slightly corrugated and distorted square nets, leading to cavities filled with unprecedented B_2C_4 finite chains, disordered C_3 units and isolated carbon atoms. Structural and theoretical analysis suggests the ionic formulation $(RE^{3+})_{15}([B_2C_4]^{6-})_3([C_3]^{4-})_2(C^{4-})_2 \cdot 11\bar{e}$ with rare-earth metals not fully oxidized. Accordingly, density functional theory calculations indicate that the title compounds are metallic

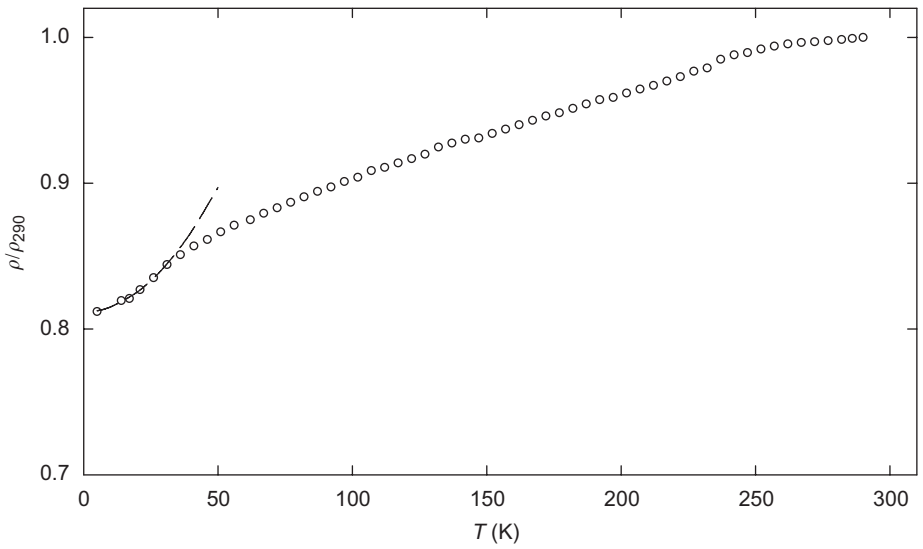

Fig. 7. Electrical resistivity vs. temperature for $Nd_{15}B_6C_{20}$.

in character. This is supported by electrical measurements carried out on $Nd_{15}B_6C_{20}$. Energy calculations on different boron vs. carbon distributions in the B_2C_4 chains support a sequence CBCCBC deduced from the X-ray structure analysis. The magnetic properties of both Pr and Nd compounds are governed by the onset of magnetic ordering at low temperatures ($T_N = 8$ K and $T_C \approx 40$ K, respectively). The results of the electrical resistivity measurements prove the ferromagnetic ground state of the Nd compound.

Supporting information

The crystallographic files in CIF format for $Pr_{15}B_6C_{20}$ and $Nd_{15}B_6C_{20}$ have been deposited with FIZ Karlsruhe as CSD numbers 418625 and 418626, respectively. These data may be obtained free of charge by contacting FIZ Karlsruhe at fax: (+49) 7247 808 666 or email: crysdata@fiz-karlsruhe.de.

Acknowledgments

The authors gratefully thank M. Babizhetska for the sample preparation, H. Gärttling for X-ray intensity data collection and Dr. J. Bauer (Université de Rennes 1) for helpful discussions. JFH and KH acknowledge support from the Austrian (ÖAD)-French (MAE) Amadeus exchange program under Projects 9/2005 (Austria) and 08940YH (France).

References

[1] J. Bauer, J.-F. Halet, J.-Y. Saillard, Coord. Chem. Rev. 178–180 (1998) 723–753 and refs. therein.
[2] J.-F. Halet, in: M.G. Davidson, A.K. Hugues, T.B. Marder, K. Wade (Eds.), Contemporary Boron Chemistry, Royal Society of Chemistry, Cambridge, 2000, p. 514 and refs. therein.
[3] M. Ben Yahia, J. Roger, X. Rocquefelte, R. Gautier, J. Bauer, R. Guérin, J.-Y. Saillard, J.-F. Halet, J. Solid State Chem. 179 (2006) 2779–2786 and refs. therein.
[4] V. Babizhetskyy, Hj. Mattausch, A. Simon, IXth International Conference of Intermetallic Compounds, L'viv, Ukraine, 2005, 20–24 September, P31.
[5] V. Babizhetskyy, Hj. Mattausch, A. Simon, 15th International Symposium on Boron, Borides and Related Compounds (ISBB'05), Hamburg, Germany, 2005, 21–26 August, I-A-2.
[6] O. Oeckler, J. Bauer, Hj. Mattausch, A. Simon, Z. Naturforsch. 59b (2004) 1551–1562.
[7] V. Babizhetskyy, Hj. Mattausch, A. Simon, Z. Kristallogr. 221 (2006) 1.
[8] P. Villars, L.D. Calvert, Pearson's Handbook of Crystallographic Data for Intermetallic Phases, second ed, ASM, Materials Park, OH, 1991.
[9] E. Bidaud, K. Hiebl, R. Hoffman, R. Pöttgen, C. Jardin, J. Bauer, R. Gautier, P. Gougeon, J.-Y. Saillard, J.-F. Halet, J. Solid State Chem. 154 (2000) 286–295.
[10] L.G. Akselrud, Yu. N. Grin, P. Yu. Zavalii, V.K. Pecharskii, WinCSD—universal program package for single crystal and/or powder structure data treatment, Materials Science Forum 335 (1993) 133.
[11] A. Altomare, M.C. Burla, M. Camalli, B. Carroccini, G.L. Cascarano, C. Giacovazzo, A. Guagliardi, A.G. Moliterni, G. Polidori, R. Rizzi, J. Appl. Crystallogr. 32 (1999) 115–119.
[12] G.M. Sheldrick, SHELXL-97: Program for the Refinement of Crystal Structures, University of Göttingen, Germany, 1997.
[13] L.J. Farrugia, J. Appl. Crystallogr. 32 (1999) 837–838 WinGX-version 1.70.01.
[14] L.M. Gelato, E. Parté, J. Appl. Crystallogr. 20 (1987) 139–143.
[15] K. Brandenburg, DIAMOND Version 2.1e, Crystal Impakt Gbr, Bonn, Germany, 1996–2001.
[16] (a) O.K. Andersen, Phys. Rev. B 12 (1975) 3060–3083;
(b) O.K. Andersen, Europhys. News 12 (1981) 4–8;
(c) O.K. Andersen, in: P. Phariseau, W.M. Temmerman (Eds.), The Electronic Structure of Complex Systems, Plenum Publishing Corporation, New York, 1984;
(d) O.K. Andersen, O. Jepsen, Phys. Rev. Lett. 53 (1984) 2571–2574;
(e) O.K. Andersen, O. Jepsen, M. Sob, in: M. Yussouf (Ed.), Electronic Band Structure and its Application, Springer, Berlin, 1986;
(f) H.L. Skriver, The LMTO Method, Springer, Berlin, 1984.
[17] U. von Barth, L. Hedin, J. Phys. C 5 (1972) 1629–1642.
[18] O. Jepsen, O.K. Andersen, Z. Phys. B: Condens. Matter 97 (1995) 35–47.
[19] P.E. Blöchl, O. Jepsen, O.K. Andersen, Phys. Rev. B. 49 (1994) 16223–16233.
[20] (a) R. Hoffmann, J. Chem. Phys. 39 (1963) 1397–1412;
(b) M.-H. Whangbo, R. Hoffmann, J. Am. Chem. Soc. 100 (1978) 6093–6098.
[21] G.A. Landrum, YAeHMOP-Yet Another extended Hückel Molecular Orbital Package, release 2.0, 1997.
[22] O. Oeckler, J. Bauer, Hj. Mattausch, A. Simon, Z. Anorg. Allg. Chem. 627 (2001) 779–788. See also;
J. Bauer, O. Bars, J. Less-Common Met. 83 (1982) 17–27;
J. Bauer, O. Bars, J. Less-Common Met. 95 (1983) 267–274.
[23] V. Babizhetskyy, Hj. Mattausch, A. Simon, Z. Anorg. Allg. Chem. 632 (2006) 2115.
[24] P. Gougeon, J.-F. Halet, D. Ansel, J. Bauer, Z. Kristallogr. 211 (1996) 823.
[25] R. Pöttgen, W. Jeitschko, Inorg. Chem. 30 (1991) 427–431.
[26] Hj. Mattausch, T. Gulden, R. Kremer, J. Horakh, A. Simon, Z. Naturforsch. 49b (1994) 1439–1443.
[27] M. Atoji, J. Chem. Phys. 46 (1967) 1891–1901.
[28] M. Atoji, J. Solid State Chem. 26 (1978) 51–57.
[29] (a) D. Ansel, J. Bauer, F. Bonhomme, G. Boucekkine, G. Frapper, P. Gougeon, J.-F. Halet, J.-Y. Saillard, B. Zouchoune, Angew. Chem., Int. Ed. 35 (1996) 2098–2101;
(b) J. Bauer, G. Boucekkine, G. Frapper, J.-F. Halet, J.-Y. Saillard, B. Zouchoune, J. Solid State Chem. 133 (1997) 190–194.
[30] K.H.J. Buschow, Handbook of Ferromagnetic Materials, vol. 1, 1980, 297pp.
[31] T. Kasuya, Prog. Theor. Phys. 22 (1959) 227–246.